Laser powder bed fusion fabrication and characterization of crack-free aluminum alloy 6061 using in-process powder bed induction heating

Syed Zia Uddin[1,2], David Espalin[1,2], Jorge Mireles[1*] Philip Morton[1,2], Cesar Terrazas[1,2], Shane Collins[1†], Lawrence E. Murr[1,3], Ryan Wicker[1,2]

1. W.M. Keck Center for 3D Innovation, University of Texas at El Paso, El Paso, TX, USA
2. Mechanical Engineering Department, University of Texas at El Paso, El Paso, TX, USA
3. Metallurgical, Materials and Biomedical Engineering Department, University of Texas at El Paso, El Paso, TX, USA

Corresponding author: Syed Zia Uddin; suddin@miners.utep.edu

Abstract

A parameter development study for pre-alloyed aluminum alloy 6061 (AA6061) was carried out using an open-architecture powder bed laser melting (LM) technology with capabilities of induction heating for raising the powder bed temperature. Cube specimens (10 mm on each side) were used for parameter development with variation in laser power and scanning speed, whereas layer thickness, hatch spacing and powder bed temperature were empirically determined. While higher relative densities were achieved when using induction heating (as compared to specimens fabricated without induction heating), the key difference in the experiments was the ability to fabricate specimens without cracks when using induction heating. That is, crack-free AA6061 parts were fabricated with the highest relative density measured of 98.7%. Micrographs of specimens fabricated with the induction heating demonstrated the lack of melt pool and melt track features, which are normally only achieved with post-processing heat treatments. This research was important in its approach of using high temperature heating of the powder bed prior to laser scanning to produce crack-free AA6061 parts. Further investigations are ongoing to explore and optimize this fabrication process.

Keywords: aluminum alloy 6061, laser melting powder bed fusion, crack-free, induction heating, high density

1 Introduction

The combined use of aluminum, titanium, and carbon fiber materials enables the aerospace industry to produce efficient (in terms of weight and cost) commercial and military aircraft. For instance, the Boeing 787 is composed of 50% (by weight) composites, 20% aluminum, 15% titanium, 10% steel, and the remainder is other materials [1]. Although the use of aluminum has decreased when compared to its predecessor Boeing 777 (down from 50%), aluminum still plays a critical role in most leading edges of the aircraft body as well as the tail and horizontal stabilizers. Processing of aluminum alloys with additive manufacturing (AM) technologies, using either

[*] Currently employed by Arconic, Austin,TX
[†] Currently employed by CalRAM Inc., Camarillo, CA

powder bed fusion or directed energy deposition processes, therefore will be important for the fabrication of legacy and upcoming aircraft parts.

Laser melting (LM) is a powder bed fusion AM process that uses a scanning laser to selectively melt metal powders. The scanning speed of the laser can be up to 3500 mm/s and the typical metal powder particle size is a distribution between 15 to 60µm. Like with other powder bed fusion AM processes, a fresh coating of powder is supplied for each layer until the complete part is produced. Specifically, for aircraft applications, LM could offer tremendous benefits for the fabrication of structural fuselage members using aluminum alloy 6061 (AA6061). Some examples of these components include stringers, bulkheads, longerons or ribs that support and transfer the aerodynamic loads imposed on the skin, to the fuselage [2]. Although AA6061-T6 already provides good formability, the combination of topology optimization and LM AM fabrication can lead to stiffer and lightweight engineered fuselage components that offer weight reductions and increased fuel efficiency.

A recent development for LM machines is the inclusion and operation of heating elements for raising the temperature of the powder bed (i.e., start plate, un-melted powder, and laser consolidated powder) during fabrication. These heating capabilities vary amongst machines, but generally can produce temperatures in the range of 200ºC (for SLM Solutions machines) to 1000ºC (for the AconityONE machine) by using either resistance or induction coils. In the current work, the use of induction heating is investigated for the processing of AA6061. Other aluminum alloys relevant to the aerospace industry and that may benefit from AM processing include AA2014, AA2017, AA2024, AA2219, AA5083, AA7050, AA7075, AA7150, AA7178, and AA7475 [3].

The AA6061 alloy is a heat treatable material primarily composed of aluminum, silicon and magnesium with small amounts of iron, copper, chromium, zinc, manganese and titanium. Common applications of the material include construction of aircraft and automobile components. Traditionally, AA6061 is cast into an ingot shape and then shaped using rolling, forging or extrusion. The alloy offers good machinability and weldability with proper filler material although with a reduction in maximum tensile strength down to that of annealed condition, which is 120 MPa from tempered strength of 210 MPa. However, traditional shaping techniques such as rolling, forging and extrusion have not fully realized complex geometries while taking advantage of the desirable combination of high strength-to-weight ratio, corrosion resistance, and thermal conductivity (as high as 167 W/m-K) that aluminum 6061 offers. That is, traditional shaping techniques have not been able to create complex internal cavities, conformal cooling, and thin features. Moreover, casting of AA6061 is difficult due to hot tearing and hot cracking. AA6061 is susceptible to hot tearing [4] due to a large $\Delta T = (T_{liquidous} - T_{solidous})$ value of 70 K [5]. Another source of crack formation is hot cracking. Hot cracking has established correlation with alloy composition [4]. AA6061 fell within the Al–Mg–Si–Fe–Ti system. The system was reported to have a maximum hot cracking susceptibility at 0.3–0.4% Fe, 0.5% Mg, 0.5% Si, and 0.15% Ti [6] which is precisely close to AA6061 as the composition in Table 1 suggests.

The processing of AA6061 has been tried with powder bed LM, laser sintering (LS), and ultrasonic consolidation. LS and LM are from the same genre, and LS could be considered as prologue to LM. Laser processing of aluminum and its alloys has always been difficult because of the high reflectivity (e.g., R = 0.75 at 1070 nm wavelength for aluminum [7]) and low absorptivity of laser, high thermal conductivity, and high coefficient of thermal expansion. Since surface area

is higher in powder when compared to flat sheets, powder bed LM of precursor AA6061 is more challenging, and the chance of oxidation is greater because greater surface area enhances different transport phenomena. Also, moisture pick up of the powder results in an increase of H_2 content in the powder. Both oxidation and hydrogen inclusion result in porosity within the fabricated part [8].

Prior to LM, indirect laser sintering (LS) was employed for layer-wise manufacturing of aluminum parts. In indirect LS, the structural metallic material was mixed with a binder, and the mixture was selectively laser sintered to produce the green part, which was post-processed for further densification. Sercombe *et al.* [9] demonstrated indirect LS of AA6061 as base material and 10 volume % of nylon as binder material. The green part was only 50% dense and was only good enough for handling, which was suggestive of low strength. Before infiltration with a second aluminum alloy for improving density, an intermediate stage of heat treatment and nitriding was necessary to give enough strength for infiltration. After infiltration, there had to be a tradeoff between ductility and strength based on the infiltrates used. A relative density of 95% was reported after all the post processing. Therefore, it could be argued that the part fabricated by indirect-LS of AA6061 suffered from lower strength while green and inclusion of infiltrates after densification.

Louvis *et al.* [10] carried out LM of AA6061 and AlSi12 using two MCP Realizer laser machines: one with a 50W laser and the other with a 150W laser. Scanning speed was varied between 80 to 420 mm/s and a range of hatching distances was used starting from 0.05mm to 0.3mm. For hatch spacing greater than 0.3mm, delamination was reported whereas hatch spacing smaller than 0.1mm resulted in low relative density. A highest of 89.5% relative density was achieved using the 150W laser power at a scanning speed of 200mm/s and hatch spacing of 0.1mm. For all the experiments, layer thickness was set to 45µm. Oxide film formation between hatches was observed. In addition, fragments of upper surface oxide film were observed between layers, which were broken and stirred (due to the Marangoni effect) during the melting of subsequent layers. Oxide film formation was identified as the major challenge in processing aluminum.

Loh *et al.* [11] conducted single track scanning of AA6061 powder using a Gaussian distributed Yb:YAG laser. Melt pool width and penetration depth (i.e. melt pool depth) were investigated using optical microscope. Also, a numerical model considering the volume shrinkage and volume fraction lost was created to relate the laser power and scan speed with melt pool geometry, melting and evaporation of powders, and temperature change [11]. They concluded that melt penetration and width would be highest at lower power and higher scanning speeds. Melt height would be highest with smaller laser powers and higher scanning speeds, although speed had a smaller effect in the case of melt height than on melt penetration and width. An increase in laser power also resulted in greater evaporation of the powder, although increasing the laser power did not increase the volume of solidified molten powder, which implied that increasing laser power would not necessarily improve the build rate.

Loh *et al.*[12] also studied the effect of beam profile on melt track in terms of melt width and penetration. During their experiments, powder bed was preheated to 100ºC. Cube specimens (10 mm on each side) made of aluminum alloy 6061 with a reported 95% relative density were fabricated using a Gaussian beam profile with a spot diameter of 80µm and a uniform (i.e., not Gaussian) beam diameter of 730 µm. Highest power for the Gaussian beam was 400W and that for the uniform beam profile was 1000W. Due to large spot diameter, energy density in case of the

Table 1 Typical chemical composition limits[I,II,III] of aluminum 6061 [ASTM B308/B308M]

	Si	Fe	Cu	Mn	Mg	Cr	Zn	Ti	Other (each)[II]	Other (total)[II]	Al
AA6061	0.04-0.8	0.7	0.15-0.40	0.15	0.8-1.2	0.04-0.35	0.25	0.15	0.05	0.15	remainder

I) where single units are shown, these indicate the maximum amounts permitted

II) other includes all unlisted metallic elements

III) total shall be the sum of unspecified metallic elements 0.010 % or more, rounded to the second decimal before determining the sum

uniform beam was smaller. A melt width greater than the spot diameter was observed in case of the Gaussian beam. Conversely, a smaller melt width than the spot diameter was observed with the uniform beam. This observation was related back to the energy density of the beam profile. It was suggested that a uniform beam could be used to hatch cross-sections due to the facility of a larger melt pool whereas the Gaussian beam could be used near the perimeter to maintain dimensional accuracy due to a smaller melt pool width. Although the authors did not acknowledge the presence and cause of microcracks, images presented in the paper included micrographs with microcracks along the build direction. Fulcher *et al.* [13] compared direct metal laser sintering of AlSi10Mg and AA6061, and they reported crack and porosity formation in AA6061. Raising build platform temperature was suggested to alleviate cracking drawing similarity with casting process. In general, LM of AA6061 attempts found in the literature suffered from low relative density, high porosity and crack formation.

The objective of this work was to identify a parameter window for LM AA6061 such that fabricated parts did not exhibit cracking and relative density was high. A critical research element in this work was the use of induction heating to preheat the powder bed prior to and during laser melting. It was identified that preheating the powder bed and maintaining at a high temperature through the fabrication process was a key differentiator in mitigating microstructure cracks. This work demonstrates unprecedented LM AA6061 coupons without cracks while maintaining relatively high relative densities (>98%). Columnar grain growth was observed in the build direction (i.e. in the vertical plane of the build platform). Further, the heat affected zone (HAZ) represented by melt pool and melt track formation was avoided using powder bed heating. LM fabrication approaches presented in this paper can be broadly applied to other metals prone to cracking such that the class and versatility of materials offered for LM will increase dramatically.

2 Materials and Methods

2.1 Powder

Gas atomized AA6061 powder (typical chemical composition as reported in [14] is listed in Table 1) was acquired from LPW Technologies (Pittsburgh,PA) in vacuum sealed containers with a silica gel pouch inside to prevent oxidation and moisture pick up. To avoid detrimental effects of humidity adsorption, the powder was stored with the silica gel pouch all the time except during the time of fabrication. The AA6061 powder was characterized in the lab to determine apparent density, flowability and powder morphology. Apparent density and flowability were

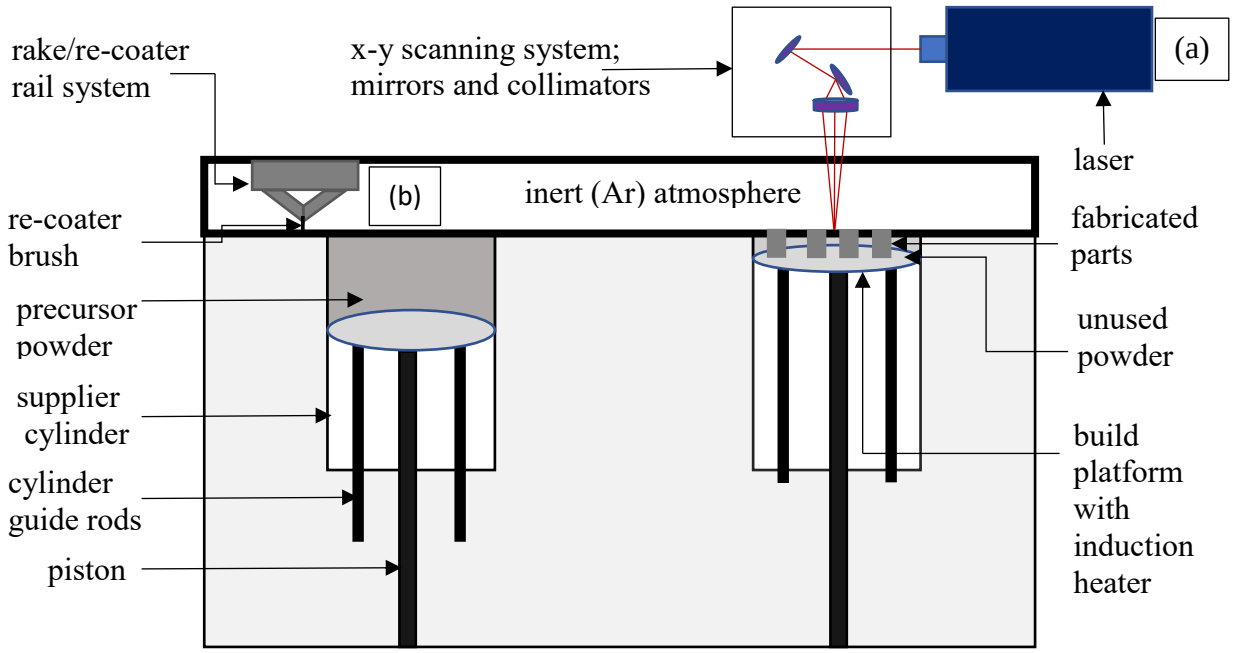

Fig. 1 A schematic representation of the AconityONE laser melting system used for the study. (a) Ytterbium fiber laser of capacity 1kW and an induction heater (not shown in figure) underneath the build platform that can raise the powder bed temperature to 1000ºC are featured. (b) The re-coater brush is made of carbon fiber to impart flexibility and high heat resistance.

measured according to method 1 of ASTM standard B212 – 09 [15] and B213 – 17 [16] , respectively.

2.2 Fabrication

An open-architecture powder bed LM machine (AconityOne, Aconity3D, Aachen, Germany) was used to fabricate 16 specimens in each build sequence. The LM machine (schematic shown in Fig.1) was equipped with a 1kW laser (Gaussian beam profile), a build chamber fed with argon inert gas, an induction coil to heat the powder bed, and a fume extraction system. Cube specimens (10 mm on each side) were fabricated (with and without induction heating of the powder bed) at different energy densities by adjusting the relevant parameters such as laser power, scan speed, hatch spacing, powder bed temperature, and layer thickness. However, the effect of induction heating was yet to be accounted for in the volume based energy density equation. As shown in Fig. 2, two parameters could be studied in a single iteration while keeping the other variables the same. An exhaustive description of all the iteration process is beyond the scope this article and a full-fledged statistical study is still underway. The two most relevant experiments to demonstrate crack-free LM fabrication of AA6061 involved exploring the empirically determined energy density space between 12.5 J/mm^3 and 25.5 J/mm^3. Fabrication was carried either without induction heating (i.e., powder bed did not receive thermal input in addition to the heating that occurs during laser melting) or with induction heating (i.e., powder bed received thermal input from both induction heating and the heating that occurs during laser melting). One specimen was fabricated for each parameter combination.

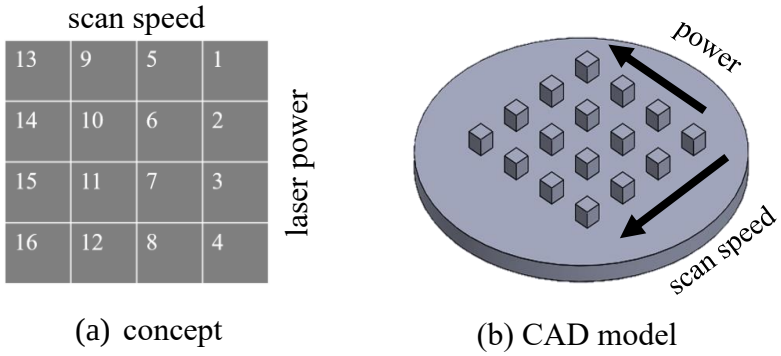

Fig. 2 Layout of the specimens and their interaction with the varied LM parameters, (a) experiment concept, (b) CAD model. Representative parameters Laser power(LP) and scan speed are shown. Other variables adjusted to obtain desired energy densities were hatch spacing and layer thickness under the external influence from induction heating of the powder bed.

2.3 Characterization

Fabricated specimens were removed from the start plate using a vertical band saw. The cube specimens were measured for density per ASTM standard B311 – 17 [17] using the volume displacement method with a weighing scale (0.001 g accuracy) (Sartorius M-prove AY303, IL, USA). The following equation was used for density (*D*) measurements,

$$D = \frac{A * E}{A - F}$$

where *A* and *F* are the measured weights for the specimen in air and water, respectively. The value of *E* is the density of the distilled water at the working temperature obtained from tabulated values provided in the B311-17 standard. Three measurements were obtained for each part. Values for the percent relative density (%RD) were calculated by dividing the density for LM-fabricated AA6061 parts into the density of wrought AA6061, which has a nominal density of 2.7 g/cm^3.

Subsequently, each specimen was cross-sectioned using a diamond-water precession cutter (TECHCUT 5^{TM}, Allied High-Tech Products, Inc, Compton, CA) along the horizontal and vertical directions. The specimens were mounted on standard 31.8 mm mounts. Sectioned specimens were ground using SiC abrasive paper starting with a 320-grit size and followed up to 1200-grit size using standard increments. Subsequent polishing was performed using Al_2O_3 particles of 3µm, 1µm and 0.05µm. To reveal the microstructure, specimens were etched for 25 seconds with an etchant with a composition as shown in Table 2. Metallographic samples were prepared following

Table 2 Composition of the customized etchant used for LM-fabricated AA6061 specimens

Component	Volume (ml)
Methanol	25
Hydrochloric acid	25
Nitric acid	25
Hydrofluoric acid	1

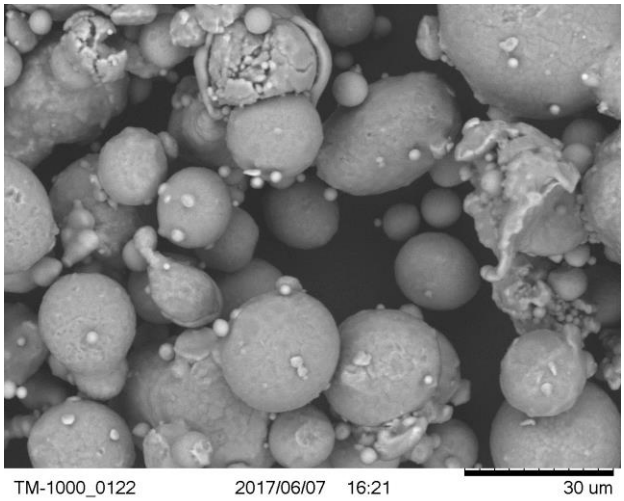

Fig. 3 SEM image of gas atomized AA6061 precursor powder. Powder shape was identified as predominantly spherical with satellites. Some non-spherical (irregularly shaped) particles were also observed.

the procedures mentioned in an article by Vander Voort [18]. Optical light micrographs were obtained using an inverted metallographic system (MEF4 A/M, Leica Microsystems, Wetzlar, Germany).

3 Results

3.1 Powder characterization

The AA6061 powder's apparent density was 1.4 g/cm^3 (Table 3), which was on the higher end of the published range (0.8 – 1.3 g/cm^3 [19]). The measured flow rate can also be found in Table 3. As shown in Fig. 3 the AA6061 powder used for the current study was predominantly spheroidal with satellites. The particle size range, which influences packing density, was reported by the powder supplier to be within 20 to 63 µm.

3.2 Fabrication and density

Fig. 4 shows LM-fabricated AA6061 cubes still attached to the build plate. Each of the cubes correspond to a different parameter set. Triangular support structures towards the bottom of the cubes, are also visible. The X and Y axis in the build plate kept track of the scan orientation. During fabrication without the induction heater, the maximum measured relative density was 98.50% (see Fig. 5) and the range was 7.31%. With the induction heater, the maximum relative density was 98.7% and the range was 2.63%. These results indicated that with the use of induction heating, not only was the maximum relative density increased, but the range was decreased. This further indicates that induction heating enables higher densities even when operating within a

Table 3: Apparent density and flow rate of the precursor powder

	apparent density (g/cm^3)	flow rate (s/50 g)
gas atomized AA6061 powder	1.4	77.74

Fig. 4 LM-fabricated AA6061 cube parts (10 mm on each side) attached to the build plate (a). A closer view of one of the specimens is offered in (b).

larger parameter space. Quantitatively, the range was decreased by 4.68% (or 64% reduction) when the induction heater was implemented. As mentioned earlier, replication studies are underway to statistically corroborate these findings.

When the induction heater was not used, the highest relative density (98.50%) was measured when the energy density was 22.3 J/mm^3. However, it will be noted in a later section of this manuscript that these specimens contained microcracks as observed through micrographs. For this experiment (i.e. no induction heater), the relative density was observed to decrease consistently at each power setting with increasing speed. The highest relative density (98.7%) was achieved with the induction heating of the powder bed and energy density of 20.40 J/mm^3. As will be noted in section 3.3, the use of induction heating resulted in crack-free part for every

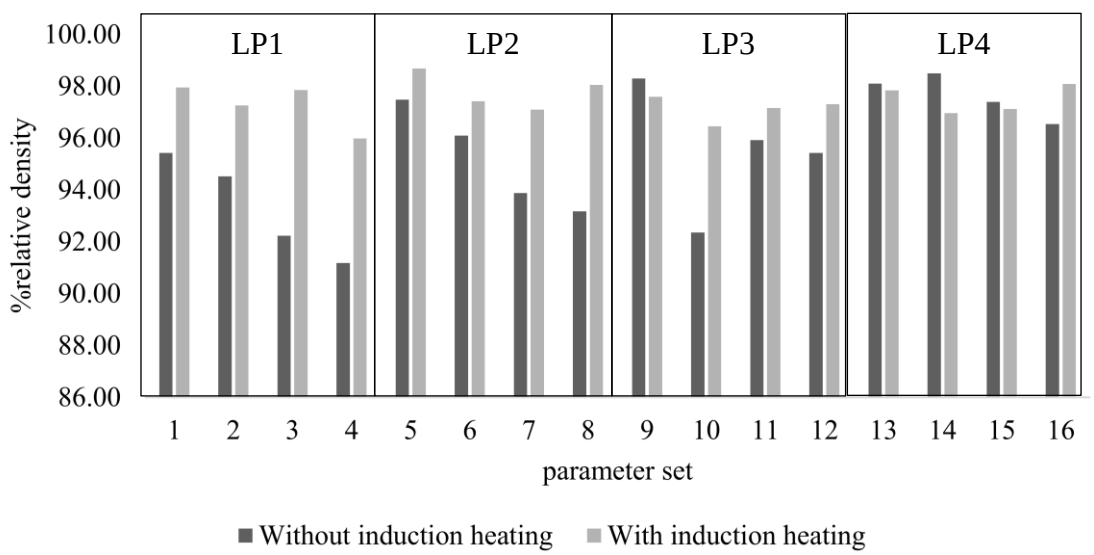

Fig. 5 The bar chart compares % relative density of LM AA6061 when fabricated with and without elevation of the powder bed temperature.

parameter combination. For experiments at laser power-1 (LP1) and LP2, the specimens built with induction heating had higher relative density, in every laser power and scanning speed combination. In the same laser power groups, the relative density was at least 1.2% higher when the induction heater was used. In addition, the highest observed difference in relative density was 5.5%. Except in the LP4 group and in parameter set 9 for LP3, the relative density was higher when using the induction heater. As noted previously, a full experimental statistical study is underway that will corroborate these findings. It will also be shown in a later section that the specimens built with the induction heater did not contain cracks within the microstructure – a research finding that to the authors' knowledge is unprecedented for powder bed laser melting of AA6061.

The volume based energy density was calculated using the following equation:

$$E = \frac{P}{v * h * t}$$

where E is expressed in J/mm^3, P is the laser power, v is the scanning velocity, h is the hatch spacing, and t is the layer thickness. Fig. 6 reports the relative density data sets presented in Fig. 5 as a function of energy density. While the induction heater's contribution to energy density was not included in these calculations, the energy density (provided only by the laser) is still presented to demonstrate the data trends and provide a comparison between the two fabrication conditions (i.e., with and without induction heater). The authors realize the importance of the induction heat contribution and have efforts in developing a method for incorporating its effect on the energy density.

Note that when the induction heater was not used, the relative density had an increasing trend (minus one outlier value) when energy density increased (Fig. 6). However, when the induction heater was used, the relative density was comparatively constant. The general increasing

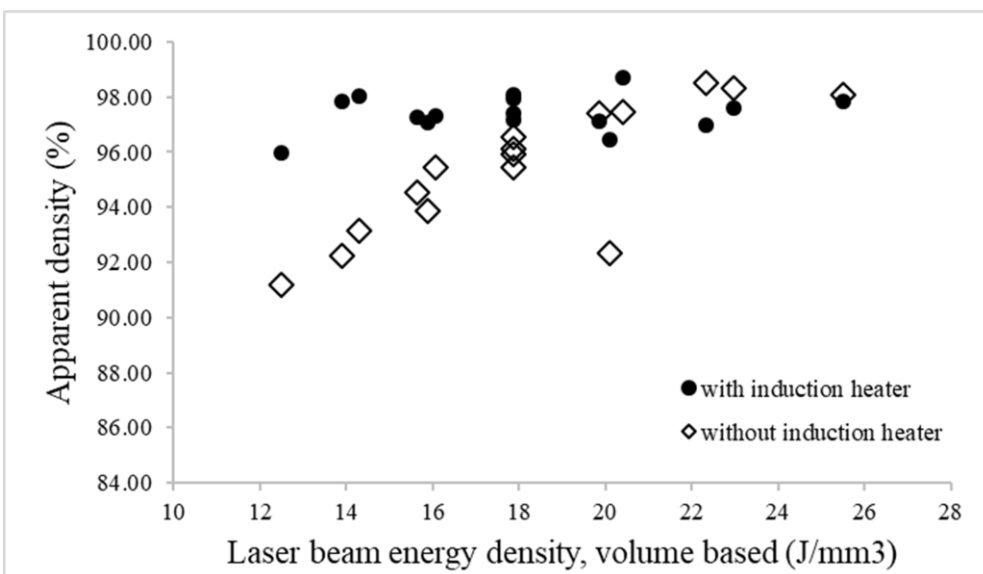

Fig. 6 Relative density (%) as a function of laser beam energy density for sample groups built with and without induction heating.

trend for the specimens fabricated without the induction heating of the powder bed appear to approach the data set of the specimens fabricated with the induction heating of the powder bed. For reference, the entire data set (all power and scanning speed combinations) for the specimens fabricated with induction heating averaged a relative density of 97.43% (n = 16, σ = 0.66), whereas the data set for the specimens fabricated without the induction heating averaged 95.40% (n = 16, σ = 2.26). Although the relative density is not as high as some reported for AlSi10Mg (99.50%) [20], the average and standard deviation for the "with induction heater" specimens highlight the induction heater's ability to broaden the parameter space and produce a low tolerance (or low standard deviation), especially compared to the "without induction heater" specimens. These

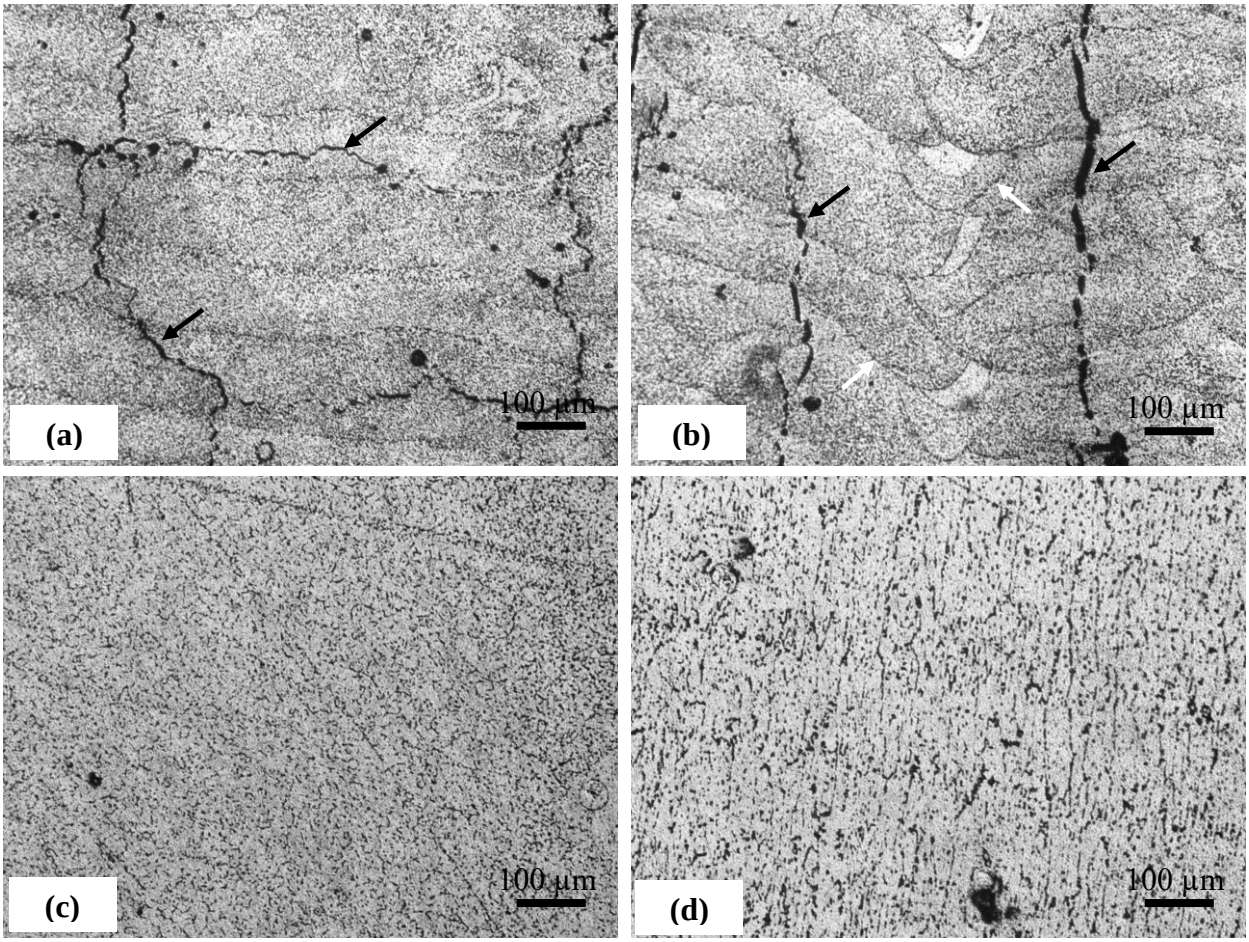

Fig. 7 Optical microscopy image of horizontal (a) and vertical (b) planes of LM-fabricated AA6061 parts "without induction heater". Also, horizontal (c) and vertical (d) planes of LM-fabricated AA6061 parts "with induction heater". Cracks (highlighted by black arrows) and melt pool tracks (highlighted by white arrows) are clearly visible in figures (a) and (b)**,** which are not present when the powder bed was heated (figures c and d). Figure (d) shows columnar grain growth that was observed in the build direction. include black "dots" probably represent precipitates formed in the build. In Fig 7d, precipitates are especially dense within the elongated boundaries

results, of course, must be corroborated by a larger data set where replicates at each parameter combination are fabricated.

3.3 Metallographic analysis

Optical light microscopy images (Fig. 7) of the horizontal and vertical planes of the specimens revealed cracks in the microstructure for the AA6061 cubes built without any induction heating of the powder. Heat affected zones were clearly visible in that case. Crack-free parts were produced when using the induction heater to raise the powder bed temperature. This was true for every specimen fabricated with the induction heater. Heat affected zones, also identified as melt pools and tracks, were not present. Instead, columnar or elongated grains were observed in the build direction. Elongated grains would result in anisotropy of properties. However, correct orientation of the elongated grains would improve mechanical property in that direction.

Porosity was observed in Fig. 7 (a) and 7 (b) in which cases the parts were fabricated without induction heating of the powder bed. The porosity can be correlated with the lower density measurements obtained for those parts. Induction heating of powder bed improved part quality by reducing porosity. Compared to Fig. 7(a) and 7(b), Fig 7(c) and 7(d) showed a noticeable reduction in the number of pores in the microscopic images although they were not removed completely.

4 Discussion

Aluminum and its alloys are known for their reflectivity of lasers and relatively high thermal conductivity (around 167 W/m-K) when compared to the other common LM material (e.g., tool steel which has a thermal conductivity of 24.3 W/m-K at 215ºC). In addition, the latent heat of fusion for aluminum (the energy required for melting) is the highest for any metal: 378kJ/kg for Al versus 297 kJ/kg for Ni and 272 kJ/kg for Fe. The corresponding latent heat of fusion/melting temperature is 0.59, 0.20 and 0.12 kJ/kg-°C for Al, Ni and Fe, respectively. Therefore, applying sufficient energy in the laser-powder bed interaction zone and keeping that energy within the melting zone has been the challenge in processing non-variant AA6061 using LM. The high relative density of AA6061 reported in this study (98.7%) when using the induction heater could be attributed to a longer life of the liquid phase in the melt zone. Metal in its powder form has a higher absorption coefficient of the laser beam due to diffuse scattering [21] . Again, laser absorptivity is a function of optical thickness and lower optical thickness means higher

Table 4 Process parameters suggested by SLM Solutions for 125HL machines

Parameters	Material		
	Titanium alloys		AlSi10Mg
Layer thickness(µm)	30	50	30
Hatch spacing(µm)	120	120	130
Power (W)	175	275	350
Scanning speed (mm/s)	775	760	1650

absorptivity [22]. The liquid phase has lower optical thickness. Therefore, it could be argued that AA6061 was least reflective to lasers in liquid form. Also, the liquid phase in general has a smaller thermal conductivity than after solidification; as a result, keeping the liquid phase longer (due to induction heating) ensured sufficient wetting of the substrate and areas around the melt track that eventually translated to higher relative density of the fabricated part.

The powder bed LM process could be regarded as a faster version of fusion welding given that in both cases full melting occurs in the fusion zone. High crack susceptibility of aluminum stems from the high solidification stresses sustained by the melt pool. Challenges increased due to high thermal expansion and thermal conductivity of AA6061. In powder bed LM, a much smaller layer thickness is used. Table 4 contains the prescribed parameter values for processing Titanium alloys and AlSi10Mg alloys using SLM Solutions 125HL machines. Highest layer thickness suggested was 50 µm. Also scanning speed between 2000 to 3000mm/s is not uncommon in laser systems. On the other hand, fusion welding uses much thicker layers of sheet, in the range of 1 to 30 mm, at a relatively slower rate of 16 to 160 mm/s, Therefore, the transient nature of the melt pool would be more dominant in the LM powder bed process than welding, hence a higher residual stress and subsequent cracking. Moreover, in welding, filler material could be introduced to change weld pool chemistry to deter cracking, which is also not possible in LM because maintaining purity of the fabricated parts is often required by the end-use application. Controlling thermal behavior by introducing a unique temperature boundary condition in LM was found to stop cracking in AA6061 fabrication. The reason for the mitigation of cracks could be attributed to stress relief from a slower solidification rate resulting from high induction heating temperature of the powder bed. The idea was supported by the fact that melt pools, melt tracks, and cracks were visible in the specimens fabricated without induction heating, whereas no heat affected zone such as melt pool or melt track were observed in the crack-free specimen produced when using the induction heater. Much work remains to fully understand the thermal behavior of the melt pool and its solidification process that deterred crack formation. Introduction of powder bed heating also holds the prospect of *in-situ* heat treatment of LM-fabricated parts.

5 Conclusion

In this research, 10 x 10 x 10 cubes of AA6061 were fabricated using laser melting (LM) with and without heating of the powder bed. Crack-free AA6061 parts were fabricated with the introduction of an induction heater that raised the powder bed temperature. A highest relative density of 98.7% was measured with elevated build platform temperature when the energy density was 20.4 J/mm^3. Heat affected zones represented by melt pools and melt tracks were also removed from the microstructure without the use of post-treatments. Instead, columnar grain growth in the build direction was observed. Results reported in this study demonstrated that crack-free fabrication of AA6061 is possible using elevated temperature LM. The concept of elevated temperature LM explored in the current study could be extended to the LM fabrication of other highly reflective and thermally conductive materials that opens the prospect of additive manufacturing to a new class of materials. Also, *in-situ* heat treatment of the fabricated parts were achieved that was enough to remove certain heat affected zone features such as melt tracks and melt pools as observed in the microstructure images.

6 Future Work

Further research will be conducted to produce replicates and gain statistical corroboration of the results presented in this work. Future work will also concentrate on increasing the density of LM-fabricated AA6061 parts using parameter optimization and post built hot isostatic pressing. Further metallographic analysis will be performed to learn about the nature of precipitates within the grains and on the grain boundaries. Introduction of powder bed heating opens the prospect of *in-situ* heat treatment of the LM fabricated part which will be explored in future research. To determine mechanical properties, tensile bars will be printed using AA6061 and heat treated to T6 condition. Building of tall parts and conduction of heat through the part bed will need to be researched further. Different large, complex, and open cell structures will be printed to fully realize the advantages of LM of AA6061. Thin features such as thin walled structure, fins, and heat sinks will be printed to extract benefit of high thermal conductivity of AA6061. As a demonstration of an end-use part, a cube-satellite frame will be printed with the goal of launching to show applicability of LM manufactured AA6061 as structural material for space applications.

Acknowledgements

The research presented here was conducted at The University of Texas at El Paso within the W.M. Keck Center for 3D Innovation (Keck Center), a 13,000-sq. ft. state-of-the-art additive manufacturing facility. The authors are also grateful to Jose Gonzalez, Elizabeth Fabella, Mohammad Hossain, and Alfonso Fernandez for their participation and contributions. The authors acknowledge LPW Technologies (Runcorn, UK) for supplying AA6061 powder.

References

[1] J. Hale, "Boeing 787 from the ground up," *Aero,* vol. 4, *(24),* pp. 7, 2006.

[2] C. Gromer, "Sign of zodiac," *Popular Mechanics,* pp. 47, 1997.

[3] P. Rambabu *et al*, "Aluminium alloys for aerospace applications," in *Aerospace Materials and Material Technologies*Anonymous 2017, .

[4] D. Eskin and L. Katgerman, "Mechanical properties in the semi-solid state and hot tearing of aluminium alloys," *Progress in Materials Science,* vol. 49, *(5),* pp. 629-711, 2004.

[5] J. Davids, "ASM Specialty Handbook, Aluminium and Aluminum Alloys," 1993.

[6] I. Novikov, "Hot-cracking of Non-Ferrous Metals and Alloys," 1966.

[7] L. Li, "The advances and characteristics of high-power diode laser materials processing," *Optics and Lasers in Engineering,* vol. 34, *(4),* pp. 231-253, 2000.

[8] E. Olakanmi, "Selective laser sintering/melting (SLS/SLM) of pure Al, Al–Mg, and Al–Si powders: Effect of processing conditions and powder properties," *J. Mater. Process. Technol.,* vol. 213, *(8),* pp. 1387-1405, 2013.

[9] T. B. Sercombe and G. B. Schaffer, "Rapid manufacturing of aluminum components," *Science*, vol. 301, *(5637)*, pp. 1225-1227, 2003. . DOI: 10.1126/science.1086989 [doi].

[10] E. Louvis, P. Fox and C. J. Sutcliffe, "Selective laser melting of aluminium components," *J. Mater. Process. Technol.*, vol. 211, *(2)*, pp. 275-284, 2011.

[11] L. Loh *et al*, "Numerical investigation and an effective modelling on the Selective Laser Melting (SLM) process with aluminium alloy 6061," *International Journal of Heat and Mass Transfer*, vol. 80, pp. 288-300, 2015. . DOI: http://dx.doi.org/10.1016/j.ijheatmasstransfer.2014.09.014.

[12] L. Loh *et al*, "Selective Laser Melting of aluminium alloy using a uniform beam profile: The paper analyzes the results of laser scanning in Selective Laser Melting using a uniform laser beam," *Virtual and Physical Prototyping*, vol. 9, *(1)*, pp. 11-16, 2014.

[13] B. A. Fulcher, D. K. Leigh and T. J. Watt, "Comparison of AlSi10Mg and al 6061 processed through DMLS," in *Proceedings of the Solid Freeform Fabrication (SFF) Symposium, Austin, TX, USA*, 2014.

[14] ASTM B308/B308M-10 Standard Specification for Aluminum-Alloy 6061-T6 Standard Structural Profiles, ASTM International, West Conshohocken, PA, 2010, https://doi.org/10.1520/B0308_B0308M-10

[15] ASTM B212-17 Standard Test Method for Apparent Density of Free-Flowing Metal Powders Using the Hall Flowmeter Funnel, ASTM International, West Conshohocken, PA, 2017, https://doi.org/10.1520/B0212-17

[16] ASTM B213-17 Standard Test Methods for Flow Rate of Metal Powders Using the Hall Flowmeter Funnel, ASTM International, West Conshohocken, PA, 2017, https://doi.org/10.1520/B0213-17

[17] ASTM B311-17 Standard Test Method for Density of Powder Metallurgy (PM) Materials Containing Less Than Two Percent Porosity, ASTM International, West Conshohocken, PA, 2017, https://doi.org/10.1520/B0311-17.

[18] G. F. Vander Voort, *Metallography, Principles and Practice.* 1984.

[19] J. R. Davis, *Aluminum and Aluminum Alloys.* 1993.

[20] L. Hitzler *et al*, "Direction and location dependency of selective laser melted AlSi10Mg specimens," *J. Mater. Process. Technol.*, vol. 243, pp. 48-61, 2017.

[21] C. Boley, S. Khairallah and A. Rubenchik, "Calculation of laser absorption by metal powders in additive manufacturing," *Appl. Opt.*, vol. 54, *(9)*, pp. 2477-2482, 2015.

[22] M. Brandt, *Laser Additive Manufacturing: Materials, Design, Technologies, and Applications.* 2016.